Optical diagnostic study of internal and external EGR combined with oxygenated fuels of n-butanol, $PODE_3$ and DMC to optimize the combustion process of FT synthetic diesel

Wanchen Sun [a], Genan Zhu [a], Liang Guo [a], Hao Zhang [a*], Yuying Yan [b], Shaodian Lin [a], Wenpeng Zeng [a], Xin Zhang [a], Mengqi Jiang [a], Changyou Yu [a]

[a] *State Key Laboratory of Automotive Simulation and Control, Jilin University, Changchun 130025, China*

[b] *Faculty of Engineering, the University of Nottingham, Nottingham, UK, NG7 2RD*

Abstract

With the introduction of carbon neutrality target, Fischer-Tropsch (FT) synthetic fuels are coming back into the limelight as a kind of carbon-neutral fuel. However, the mismatch between the overly high cetane number (CN) and the relatively low vaporability of FT synthetic diesel is unfavorable to the soot emission control, which will make it difficult to meet more stringent fuel consumption and emission regulations in future applications. To investigate the potential of oxygenated fuels combined with different exhaust gas recirculation (EGR) introduction schemes to achieve high-efficiency and clean combustion of FT synthetic diesel, an optical diagnostic study was

* Corresponding author, Address for correspondence: State Key Laboratory of Automotive Simulation and Control, Jilin University, Changchun 130025, People's Republic of China.

E-mail address: haozhang@jlu.edu.cn (Hao Zhang).

carried out based on high-speed photography and the two-color method. The results show that all three kinds of oxygenated fuels could suppress soot emissions via self-carrying oxygen and adjusting the physicochemical properties of the fuel blend. Compared with the combustion characteristics of FT synthetic diesel, the flame area and luminosity of oxygenated blends are reduced, and the in-cylinder temperature and soot KL factor are lowered. Among them, n-butanol exhibits a greater capability of soot control compared to polyoxymethylene dimethyl ethers ($PODE_3$) and dimethyl carbonate (DMC). In addition, introducing internal and external EGR to the engine fueled by n-butanol/FT synthetic diesel blend shows that with the increase of EGR rate, the external EGR exhibits a gradually stronger inhibiting effect on the heat release process and soot KL factor, while the internal EGR exhibits an inhibiting and then promoting effect. Moreover, the high ratio internal EGR shortens the ignition delay (ID) significantly due to the strong heating effect, which is unfavorable to the control of soot emission. The combination of oxygenated fuels and internal/external EGR could effectively optimize the combustion process of FT synthetic diesel and inhibit soot generation, but the EGR rate needs to be controlled within a proper range.

Keywords: FT synthetic diesel; N-butanol, $PODE_3$, DMC; Flame characteristics; Two-color method; Internal and external EGR

Highlights:

- An optical diagnostic of optimizing FT synthetic diesel combustion was conducted.
- Blending oxygenated fuels contribute to combustion optimization and soot reduction.

- N-butanol exhibits the strongest soot-inhibiting ability followed by $PODE_3$ and DMC.
- External EGR exhibits an inhibiting effect on combustion and diffusion flame.
- Heating effect of high-rate internal EGR neutralizes its inhibiting effect.

Abbreviations

FT	Fischer-Tropsch	LII	Laser-induced incandescence
CN	Cetane number	PIV	Particle image velocimetry
CI	Compression ignition	PDPA	Phase doppler particle analyzer
ITE	Indicated thermal efficiency	ECU	Electronic control unit
COV	Coefficient of variation	MCU	Microprogrammed control unit
PPRR	Peak pressure rise rate	VVT	Variable valve timing
PHRR	Peak heat release rate	HRR	Heat release rate
R_p	Premixed gasoline ratio	IMEP	Indicated mean effective pressure
ID	Ignition delay	CR	Compression ratio
DMC	Dimethyl carbonate	RGB	Red green blue
PODE	Polyoxymethylene dimethyl ethers	SINL	Spatially integrated natural luminosity
EGR	Exhaust gas recirculation	φ_a	Excess air ratio
NVO	Negative valve overlap	SOI	Start of injection
ICE	Internal combustion engine	NVOA	Negative valve overlap angle
LIF	Laser-induced fluorescence	CD	Combustion duration

1 Introduction

Global warming is a worldwide problem for mankind. Throughout more than 150 years, human activities have produced a considerable amount of greenhouse gases into the atmosphere, causing significant impacts on the climate [1-3]. To ensure the sustainability of ecosystems and human society, the target of limiting global warming to 1.5°C has been proposed [4,5], which calls for halving carbon emissions by 2030 and achieving carbon neutrality by 2060 [6-8]. In this regard, the development of clean low/zero carbon fuels plays an important role in the decarbonization of the energy and transportation sectors [9,10], such as biofuels based on direct photosynthesis [11,12], green hydrogen/green ammonia [13,14], and e-fuels based on green electricity, etc [15,16]. Although Fischer-Tropsch (FT) synthetic diesel still has problems such as high pre-investment costs compared with other alternative fuels [17], it also has some unique advantages such as high energy density, greater compatibility with existing storage and refueling infrastructure, and adaptability to current engine technology [18].

Compared with conventional petroleum diesel, FT synthetic diesel has a higher content of straight-chain alkanes, lower sulfur, and aromatic hydrocarbons, higher cetane number (CN), better flammability, and can be miscible with conventional diesel in any ratio. These features make FT synthetic diesel a promising alternative fuel for compression ignition (CI) engines [19-21]. Many studies have shown that the use of FT synthetic diesel contributes to the optimization of combustion and emission characteristics of CI engines. Shi et al. studied the effect of FT synthetic diesel fuel on a turbocharged, intercooling, common-rail diesel engine and showed that FT synthetic diesel fuel contributed to a higher indicated thermal efficiency (ITE) and lower coefficient of variation (COV) compared to China VI diesel [22]. Zhang et al. compared the impacts of using diesel and FT synthetic diesel as pilot fuel on combustion and emission characteristics respectively in RCCI mode [23]. It showed that FT synthetic diesel with higher CN could reduce COV, control the peak pressure rise rate (PPRR) and peak heat release rate (PHRR), and expand the load range of RCCI mode under a low premixed gasoline ratio (R_p). In addition, the authors pointed out that the FT synthetic diesel fuel could reduce soot emissions, and similar conclusions were mentioned in several other studies [24-28].

The lower soot emissions of FT synthetic diesel are mainly due to the low aromatic content, which inhibits the formation of soot precursors [25,26]. However, with the improvement of commercial fuel standards, the aromatic content of fossil diesel will be gradually reduced, and the advantage of low aromatic content of FT synthetic diesel will gradually disappear, while its higher CN will lead to worse combustion timeliness and higher soot emission [29,30]. Adding oxygenated fuels with different molecular structures such as n-butanol [31,32], dimethyl carbonate (DMC) [33,34], and polyoxymethylene dimethyl ethers (PODE) [35,36] could exert the advantage of the oxygen-carrying property on inhibiting the generation of soot [37-39]. Oxygenated additives are capable of all-round combustion regulation from the physicochemical properties of the fuel, such as ignition and combustion phases, mixture stoichiometry distribution, adiabatic flame temperature, and temperature field distribution of the combustion process, etc. [40-42], so it is necessary to investigate the effect of the introduction of oxygenated fuels on the combustion process of FT synthetic fuel. Additionally, as a means of adjusting the properties of working medium, EGR also plays an important role in the combustion regulation [43-45]. Apart from external EGR which is used commonly, internal EGR is also an effective method of combustion control. Duan et al. implemented internal EGR through negative valve overlap (NVO) and investigated the effect of internal EGR on combustion and emissions of the engine

[46]. The results showed that NOx emissions were reduced but the CO and HC emissions increased as the internal EGR rate increased. It is necessary to carry out research on controlling the combustion process of FT synthetic diesel fuel by combining internal/external EGR with oxygenated fuels, however, relevant studies have been rarely reported.

As a non-intrusive research method, optical diagnostic has the characteristics of fast response, high sensitivity, and intuitive results, thus becoming an important method in the study of the working process of the internal combustion engine (ICE), such as fuel injection, vaporation, air-fuel mixing, flame development, and pollutant generation history, etc [47-49]. Recently, with the advancement of optics and materials science, a variety of optical diagnostic methods such as laser-induced fluorescence (LIF), laser-induced incandescence (LII), particle image velocimetry (PIV), Phase Doppler Particle Analyzer (PDPA) and high-speed photography have also been used in the research of ICE widely [29,50-55]. Matsui et al. introduced an optical diagnostic technique of high-speed photography combined with the two-color method based on solid thermal radiation theory [56,57], which has been improved by the researchers and is now capable of systematically studying the flame development history, in-cylinder temperature field, and soot concentration field [58-62]. Jeon et al. investigated the flame characteristics, temperature field, and soot KL factor field during the combustion of a biodiesel/diesel blend (biodiesel at 20% v/v) at various injection pressures based on the two-color method [63]. The results showed that the flame temperature and soot concentration of the oxygenated blend were higher at all the injection pressures compared to those of pure diesel. Therefore, optical diagnosis is an essential and effective research method in revealing the impacts of oxygenated fuels and internal/external EGR on the combustion and the soot generation processes during the combustion of FT synthetic diesel.

In this study, an optical diagnostic test system was built based on a single-cylinder diesel engine with flexible and adjustable combustion boundary conditions. The effects of oxygenated fuel combined with internal/external EGR on the combustion process and soot generation history were investigated using FT synthetic diesel as the base fuel. The results will be able to establish a theoretical basis for the development of high-efficiency and clean combustion strategies based on FT synthetic diesel.

2 Experimental setup and test procedure

2.1 Optical Engine Test Bench

Fig. 1 shows the layout of the optical engine measurement and control platform. The test platform consisted of optical engine, electronic control system and high-speed photography system. The optical engine was driven by an electric motor to operate steadily at a constant speed, and the engine position signal was acquired by the crankshaft and camshaft position sensors and transmitted to the control system (open electronic control unit (ECU) NI 2106). The NI system took the control of injection parameters and sent the trigger signal to the microprogrammed control unit (MCU) once per cycle. The MCU implemented the control of the high-speed camera and the hydraulic variable valve timing (VVT) system. Moreover, the real-time acquisition and analysis of the combustion state were carried out by the combustion analyzer based on the signal from the cylinder pressure transducer and the encoder. In this study, the heat release rate (HRR) was calculated based on the HRR calculation module of the combustion analyzer, which is based on the multivariate exponential algorithm and the Rassweiler and Withrow model, where the multiple variable index was chosen as 1.37 empirically. In addition, previous studies have shown that the addition of oxygenated fuels introduced in this study could lead to increased cyclic variability [64]. Considering the intensity of the optical window, the optical engine was not allowed to run continuously for a long time. To minimize the effect of cyclic variability, the cylinder pressure data was collected for 15 cycles in each working condition, and the one cycle with the indicated mean effective pressure (IMEP) closest to the average IMEP was selected as the combustion data for that working condition.

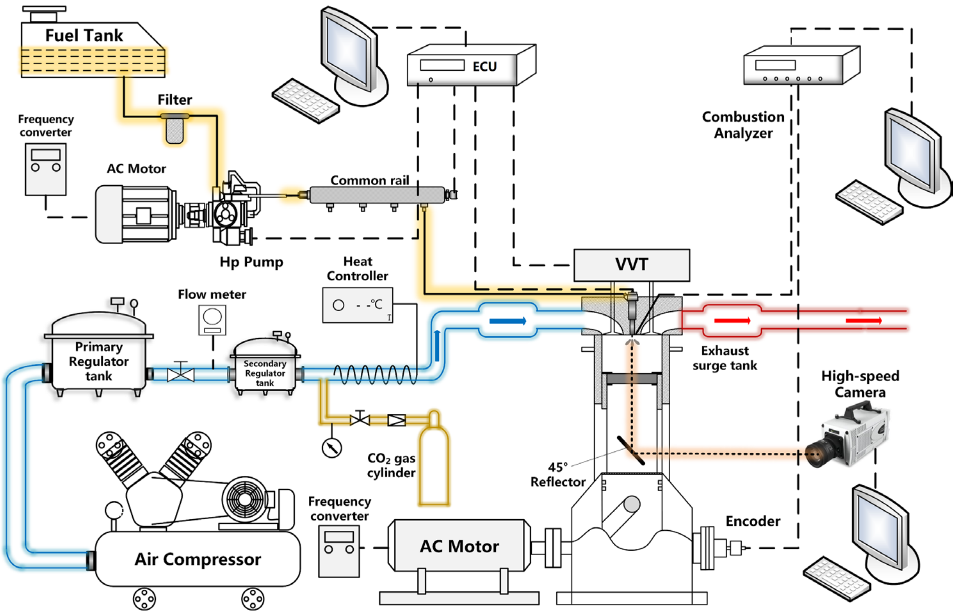

Fig. 1. Optical engine measurement and control platform.

The optical engine was modified from a single-cylinder diesel engine and the technical specifications are listed in **Table 1**. The adopted optical engine modification was the Bowditch type, with an optical window on the top of the extended piston and the lowered 45° reflector. The structure of the extended cylinder and the schematic of the optical pathway are shown in **Fig. 2**. In addition, to implement internal EGR through flexible control of valve timing, a hydraulic VVT system was adopted to replace the stock valvetrain. The original compression ratio (CR) of the optical engine is 17. Due to the shape requirements of optical glass, the piston head could only take the shape of a flat top. The flat piston head limited the CR of the optical engine to a maximum of 13. To ensure a reliable compression ignition, the temperatures of the intake air and the coolant were heated to 353 K and 363 K respectively.

Table 1 Technical specifications of the optical engine.

Category	Properties
Bore×stroke / mm	105×114.3
Connecting rod length / mm	190
Displacement / L	0.99
Geometric compression ratio	13
Valve lift / mm	11
Number of valves	4
Number of injector nozzle holes	7
Diameter of nozzle hole / mm	0.12

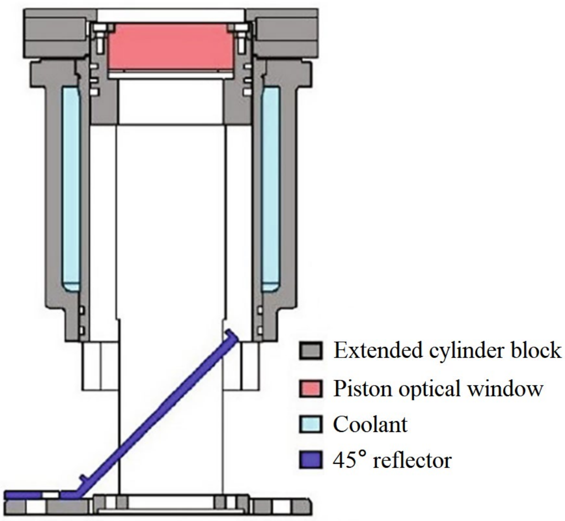

Fig. 2. Schematic of optical pathway.

2.2 High-speed photography and image processing

The high-speed camera adopted in this study was Phantom v611 produced by AMETEK, USA. The high-speed camera was operated under the external trigger mode, based on the trigger signal from ECU and the synchronization signal from the encoder to accomplish the accurate control of the sampling time. The sampling parameters of the high-speed camera are shown in **Table 2**. The natural luminescence signal of the in-cylinder flame captured under such sampling parameters mainly consisted of narrowband chemiluminescence and broadband soot incandescence. The intensity of chemiluminescence in the visible and near-infrared bands was much lower than that of soot incandescence [65], so the in-cylinder flame images could be considered as soot incandescence during diffusion combustion.

Table 2 The sampling parameters of high-speed camera

Category	Properties
Resolution	512×512
Aperture level	7
Exposure time / μs	4
Sampling interval	1°CA

The raw images captured by the high-speed camera were saved in Red Green Blue (RGB) format, and the flame images for analysis were pre-processed by cropping, denoising, and enhancing the raw images via a self-programmed MATLAB script. Each flame image was further processed by grayscale and binarization to identify the flame region, then the percentage of flame area and the flame luminosity (spatially integrated natural luminosity, SINL) were calculated [66,67]. In addition, the in-cylinder temperature field and soot KL factor field were obtained by the two-color method. The two-color method is a temperature measurement methodology developed on the basis of solid thermal radiation theory [68,69]. The transcendental equation of the two-color method was solved by Newton's iterative method, and the corresponding MATLAB script was programmed to implement batch post-processing of flame images.

The temperature measurement via the two-color method necessitated a brightness temperature calibration with a high-temperature blackbody furnace to establish the correspondence between the RGB values of the image and blackbody temperature. The calibration images at different temperatures are shown in **Fig. 3**. The RGB values of each pixel within the image were extracted and averaged to obtain the calibration data at each temperature, as shown in **Table 3**. To validate the reliability of the calculation procedure, the calibration images were computed and compared with the actual temperature. The computational errors at each temperature are shown in **Table 4**, ensuring the accuracy of the calculation procedure employed in this study.

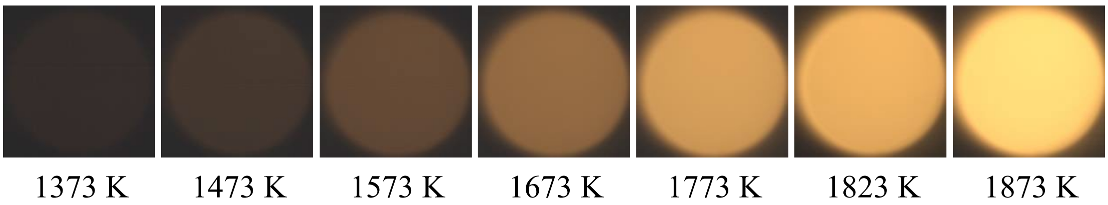

Fig. 3. The calibration images at various temperatures.

Table 3 The calibration data at various temperatures.

Temperature / K	R	G	B
1373	52.53	45.97	43.03
1473	70.28	55.95	47.07
1573	102.3	75.52	54.35
1673	150.71	109.11	67.81
1773	219.09	161.87	92.22
1823	240.3	179.54	98.48
1873	255	219.87	121.87

Table 4 The computational errors at various temperatures

Actual value / K	1373	1473	1573	1673	1773	1823	1873

Estimated value / K	1388	1468	1574	1682	1787	1815	1864
Absolute error / K	15	-5	1	9	14	-8	-9
Relative error / %	1.09	-0.34	0.06	0.54	0.79	-0.44	-0.48

2.3 Experimental plan

In this experiment, FT synthetic diesel was used as the baseline fuel which was labeled as FT. To investigate the effects of different oxygenated fuels on combustion and soot generation process of FT synthetic diesel, several FT/oxygenated fuel blends with the same oxygen content of 7.73% were adopted to ensure that the fuel-bound oxygen content would not affect the test results [70]. The chosen oxygenated fuel additives were DMC ($C_3H_6O_3$), PODE$_3$ ($C_5H_{12}O_4$) and n-butanol ($C_4H_{10}O$) with the blending mass fractions of 14.5%, 19.3%, and 35.8%, the oxygenated blends were labeled as DF, PF, and BF, respectively. In the following section, the potential of oxygenated fuels coupled with internal/external EGR to achieve the clean combustion of the CI engine was investigated based on BF. The main physicochemical properties of the test fuels are listed in **Table 5**. The heat value of the fuel being injected into the cylinder per cycle in this study was consistently controlled at 1438 J/cycle, with an IMEP of approximately 0.4 MPa. During the experiment, the engine speed was maintained at 1000 r/min, the intake mass flow and intake pressure were kept at 60 kg/h ($\varphi_a \approx 4$) and 1.8 bar (absolute pressure). The injection pressure was controlled at 100 MPa, and the start of injection (SOI) timing was fixed at -9°CA ATDC. The correspondence between injection mass and injection pulse width for each test fuel was calibrated before the experiment.

Table 5 Physicochemical properties of test fuels

Category	FT	N-butanol	DMC	PODE$_3$

Density at 20°C / ($kg \cdot m^{-3}$)	757	805.5	1069	1024.2
CN	75.4	25	35	78
Lower heating value / ($MJ \cdot kg^{-1}$)	43.07	33.1	13.5	19.05
Latent heat of vaporization / ($kJ \cdot kg^{-1}$)	~	585	369	~359 [a]
Kinematic viscosity at 25°C / ($mm^2 \cdot s^{-1}$)	2.14	3.64	0.63	1.05
Boiling point / °C	257.8	117.7	90	156
Total aromatics / %	0.8	0	0	0
Sulfur content / 10^{-6}	0.38	0	0	0

[a] Taking the latent heat of vaporization of $PODE_{3-8}$ as the reference value [71]

In this study, pure CO_2 was introduced through a gas cylinder as the simulated external EGR and the CO_2 gas was heated together with the intake air in the inlet. The selected external EGR rates in the experiment were 10%, 20%, and 30%, which were adjusted through the EGR regulating valve and air flow regulating valve. The NVO strategy was used to retain exhaust gases and thus implement internal EGR, and the valve timing was flexibly adjusted to achieve early exhaust valve closing and late intake valve opening. The selected negative valve overlap angles (NVOAs) in the experiment were 40°CA, 60°CA, 80°CA, 100°CA, and 120°CA, and the original NVOA of -28°CA was also taken into consideration.

3 Results and discussions

3.1 Effects of oxygen-containing functional group structures on the FT synthetic diesel combustion and soot generation process

The cylinder pressure, heat release rate, and combustion characteristics of the optical engine fueled with FT, DF, PF, and BF are shown in **Fig. 4**. The prolongation of the ID varies with the type of oxygenated fuel blended into FT. Among them, the CNs of $PODE_3$ and FT are similar. Compared to FT, the PF with higher latent heat of vaporization exhibits a longer ID, and the combustion starting points are delayed. Additionally, due to the high latent heat of vaporization and lower heating value of

$PODE_3$, the peak cylinder pressure and PHRR of PF are relatively low. For n-butanol and DMC, the low CNs become the dominant factor that significantly prolongs the IDs and delays the combustion process for both BF and DF blended fuels. Especially, the lower viscosity and boiling point of DMC make a stronger vaporability, so the mixture formed is more homogeneous but more fuel-lean. DF requires a longer time to reach the concentration requirement of auto-ignition, thus the ID of DF is longer than that of BF. The longer IDs for BF and DF lead to higher premixed combustion ratios and result in shorter combustion durations (CDs). However, the ID of DF is too long to maintain desirable combustion timeliness compared to that of BF. The addition of n-butanol is more appropriate to improve the combustion process of FT.

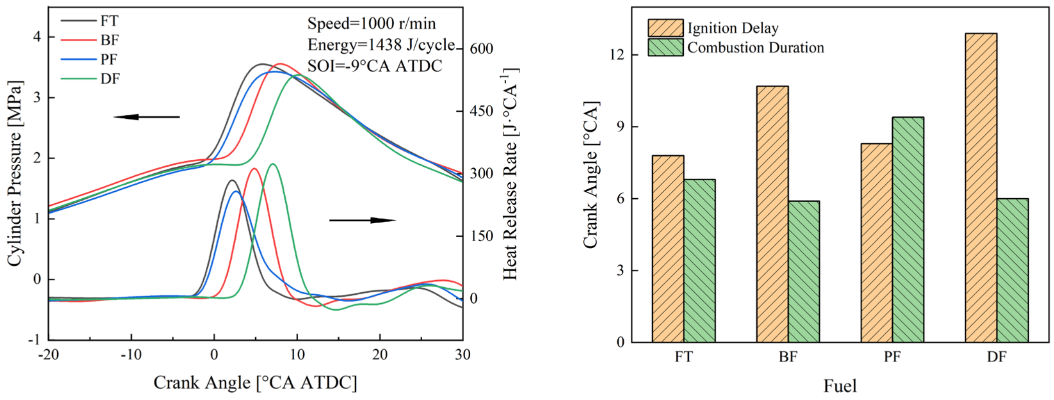

(a) Cylinder Pressure and HRR (b) Combustion characteristics

Fig. 4. Effects of oxygen-containing functional group structures on the FT synthetic diesel combustion process.

Fig. 5 and **Fig. 6** show the effects of the structures of oxygen-containing functional groups on the history of flame development and characteristic parameters of FT. As it shows in the figure, a large area of spray-shaped bright diffusion flame can be seen during the combustion process of FT because of the high CN and short ID of FT. Such a pattern of combustion makes air-fuel mixing and combustion processes highly overlapped and causes massive fuel cracking reaction under high-temperature and fuel-rich conditions [72]. Therefore, the soot generation is significantly strengthened and manifests as an extensive bright diffusion flame. During the intermediate stage of combustion, the flame distribution is then concentrated towards the cylinder wall as a result of fuel impingement. In the late stage of combustion, a punctiform flame appears around the cylinder axis and exists for a long time. It is due to the needle valve seats at the end of the injection process, resulting in the reduction of the injection pressure and the spray penetration, leading to poor atomization. Additionally, due to the weak airflow near the cylinder axis, diffusion combustion is conducted slowly by the poorly atomized fuel here. After blending oxygenated fuels, the peaks of flame area percentage and SINL are reduced significantly (FT>PF≈BF>DF), and the flame appears in the sequence of FT, PF, BF, DF. The self-carried oxygen of fuel can relieve the local fuel-rich phenomenon caused by the non-uniform distribution of air-fuel mixture, inhibit the generation of soot precursors, and promote the later oxidation of soot. Accordingly, the generation of soot is suppressed, and the flame area and luminosity of oxygenated blended fuels can be reduced. On the other hand, the introduction of oxygenated fuels could adjust the physicochemical characteristics of the blended fuels, and promote the air-fuel mixing indirectly by extending the ID and enhancing the vaporability. It can improve the premixed combustion rate, and alleviate the problem of a large proportion of diffusion combustion caused by high CN and relatively insufficient vaporability of FT. Similar to FT, the flames of PF and BF are spray-shaped as well, but the bright yellow area of PF flame is significantly smaller than FT, while BF flame shows dark yellow overall. For DF with the longest ID, due to the highest premixed combustion rate and the homogeneity of combustion, the flame is mainly concentrated along the cylinder wall without showing the shape of the fuel spray explicitly.

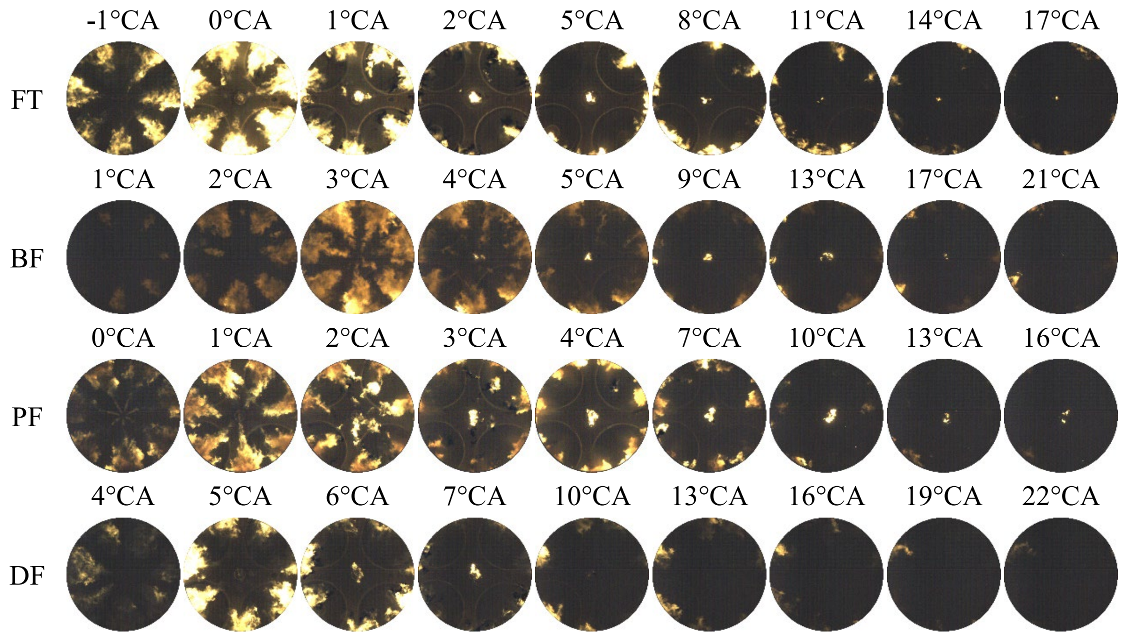

Fig. 5. Effects of oxygen-containing functional group structures on the history of flame development.

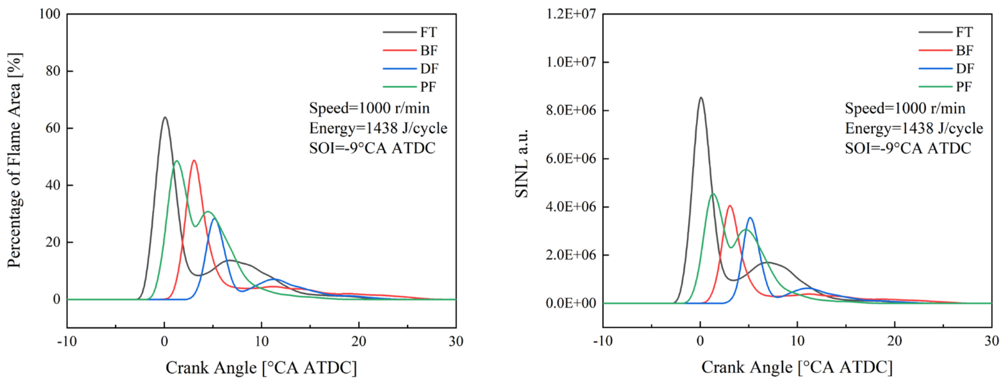

(a) Percentage of flame area (b) SINL

Fig. 6. Effects of oxygen-containing functional group structures on flame area and luminosity.

Fig. 7 and **Fig. 8** show the distributions of in-cylinder temperature fields of the four fuels. Generally, the addition of oxygenated fuel results in the mitigation of high-temperature combustion phenomenon, showing up as the reductions in the area of the local high-temperature and the number of high-temperature pixels especially the ones > 1600 K. Studies have pointed out that the main temperature range for soot formation is 1600 K-2600 K [73,74], so in order to balance thermal efficiency and soot emission control, it is necessary to minimize the area of high temperature beyond 1600 K and increase the average temperature of the area below 1600 K simultaneously, which is equivalent to increasing the temperature of the heat source in the Carnot cycle. Among the oxygenated blends, BF is the best in maintaining high thermal efficiency and avoiding the soot generation temperature range simultaneously. The overall in-cylinder temperature of the PF combustion process is lower than those of FT and BF, and the number of high-temperature pixels above 1600 K is more than that of BF. In the cloud map of temperature distribution, a large yellow and red region is present for PF, and the duration of high-temperature area presence is also prolonged, representing a more significant local high-temperature combustion phenomenon, which is not conducive to the control of soot generation. In contrast, the temperature cloud map of the BF shows a larger blue and green region and a smaller region in red, suggesting that the temperature distribution during BF combustion is more uniform. For DF, due to the delayed heat release process, the lower in-cylinder temperature and pressure caused by the down going piston resulting in a lower heat release rate. Therefore, the overall in-cylinder temperature of DF is lower than those of the other fuels, and the high-temperature pixels (> 1600 K) are numerous and mainly distributed along the cylinder wall.

-1°CA 0°CA 1°CA 2°CA 5°CA 8°CA 11°CA 14°CA 17°CA

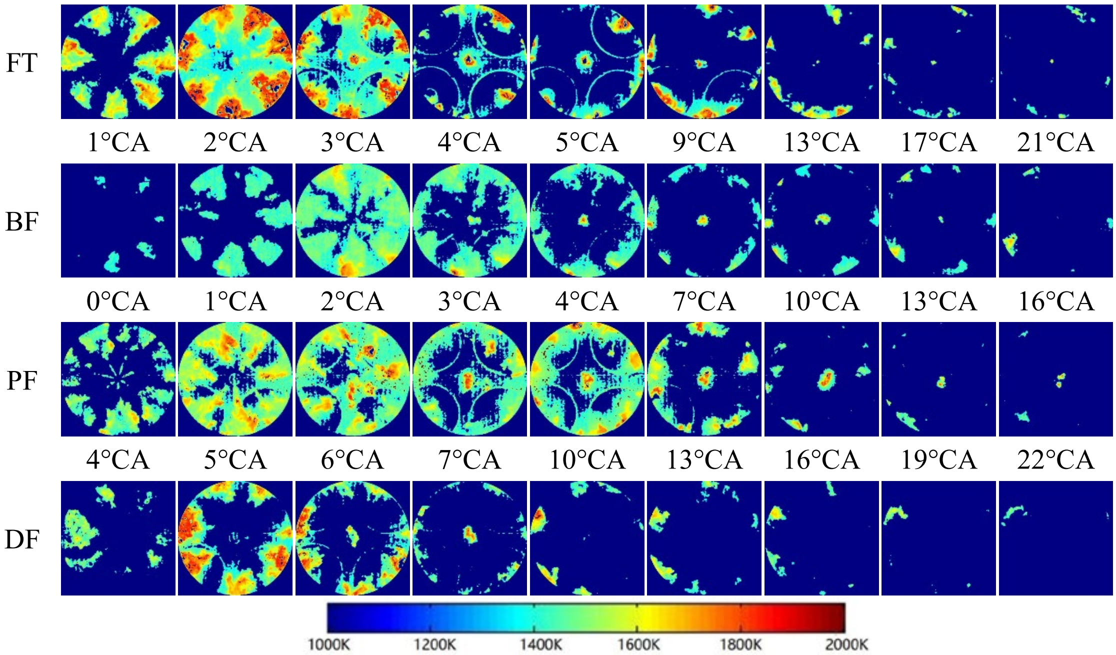

Fig. 7. The cloud maps of temperature distribution for blend fuels with different molecular structures.

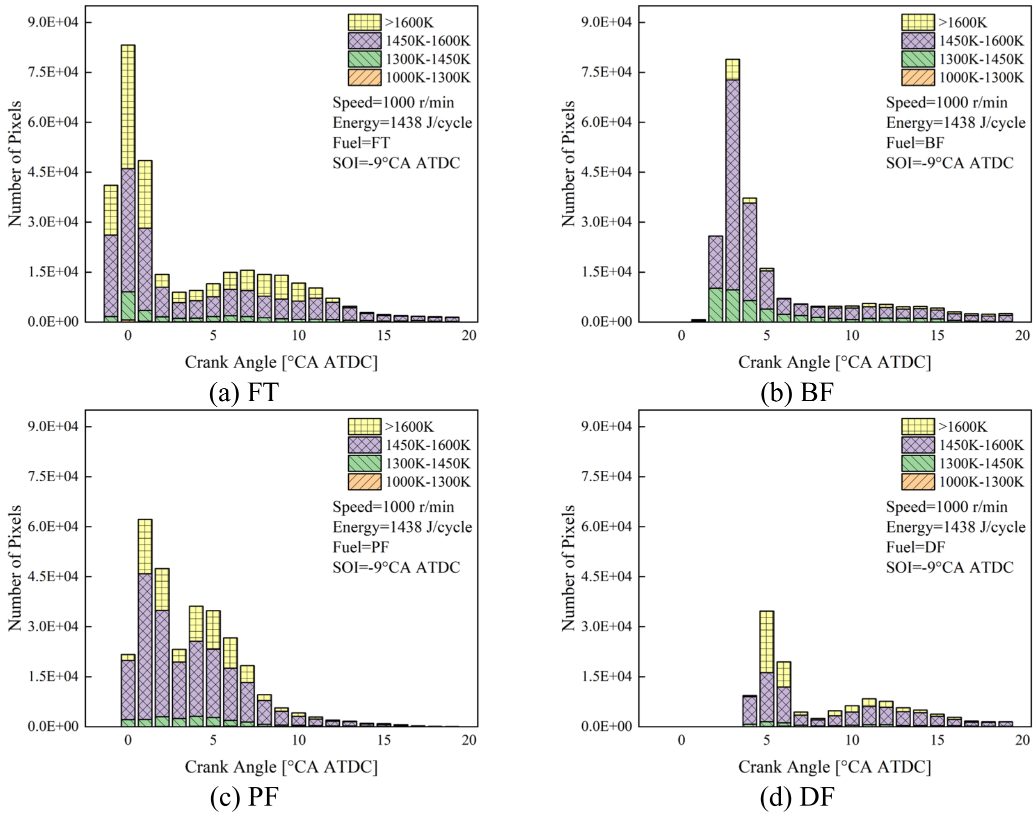

Fig. 8. The cumulative histograms of temperature distribution for blend fuels with different molecular structures.

The KL factor field distributions of the fuels are shown in **Fig. 9** and **Fig. 10**. It can be seen that the addition of oxygenated fuel can reduce the KL factor during the combustion process to varying degrees. The KL factor field is more uniformly distributed during the combustion process of BF, and the number of pixels with KL factor > 0.06 is consistently lower compared to those of the other two oxygenated blends. The KL factor of the BF reaches the peak at 3°CA ATDC and the peak is higher than the peaks of the other two oxygenated blends, but the KL factor decreases rapidly as the combustion proceeds. Although the peak KL factor of PF is lower than that of FT and BF, the duration of KL factor presence is prolonged, the KL factor decreases slowly during PF combustion process. In addition, there is an area of high concentration of soot at the edges of PF flame, which is reflected in the cumulative histogram with a higher number of pixels with KL factor > 0.06. The main limiting factor for the soot reduction capability of $PODE_3$ is the excessively high CN which leads to a short ID, an overproportion of diffusion combustion, insufficient air-fuel mixing and accelerated high-temperature fuel-rich cracking reactions. As the combustion process of DF is postponed, the lower in-cylinder pressure and temperature could inhibit the generation of soot, so the overall KL factor of DF is lower. However, it should be noted that the combustion process of DF also suffers from the regions of high soot concentration, and the variation of the KL factor shows a double-peaked tendency which is similar to those of FT and PF. In summary, among the three oxygenated blends, BF has the strongest ability in inhibiting soot generation, which is consistent with the findings of other studies [75-77].

-1°CA 0°CA 1°CA 2°CA 5°CA 8°CA 11°CA 14°CA 17°CA

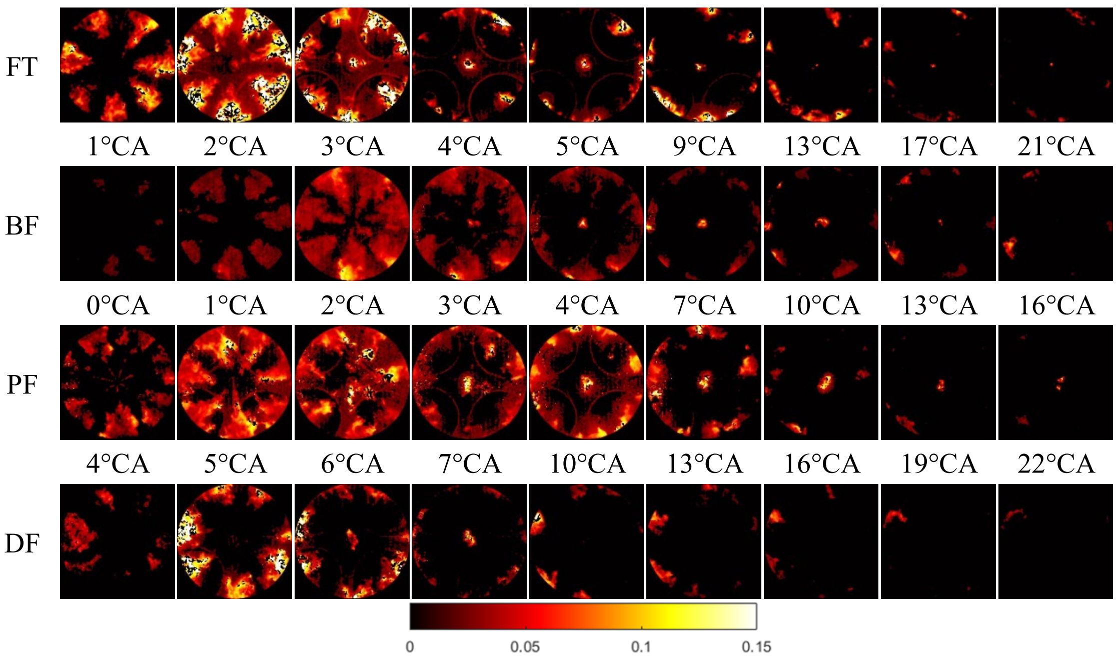

Fig. 9. The cloud maps of soot KL factor distribution for blended fuels with different molecular structures.

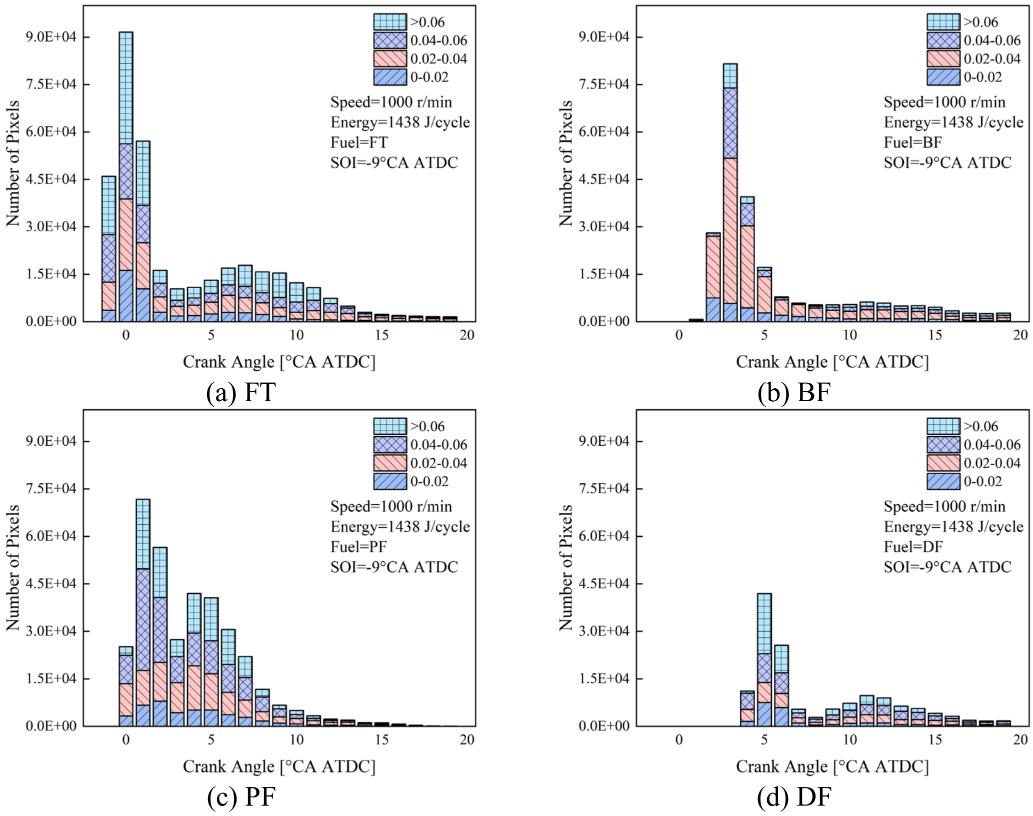

Fig. 10. The cumulative histograms of soot KL factor distribution for blended fuels with different molecular structures.

3.2 Effects of internal and external EGR on combustion and soot generation of n-

butanol/FT synthetic diesel blend

Among the three oxygenated fuels used in this study, n-butanol has the outstanding ability in the control of soot generation, and the addition of n-butanol to FT could maintain better combustion timeliness without prolonging the CD excessively, which ensures an acceptable fuel economy together with restrained soot emission. Therefore, BF is selected in this section as the test fuel to investigate the effects of different EGR introducing schemes and EGR rates on the combustion process.

Fig. 11 and **Fig. 12** show the effects of different ratios of external EGR on the flame development history and flame characteristics of BF. It can be noticed that the external EGR presents an inhibitory effect on BF combustion. As the external EGR rate increases, the percentage of diffusion flame area and the SINL decrease, the ID is prolonged, and the timing of flame appearance is significantly delayed. The cylinder temperature before combustion is decreased because of the higher specific heat of in-cylinder gas, and the reactivity of the air-fuel mixture is reduced by the decline of oxygen concentration in the cylinder [78,79], the two factors above lead to the prolongation of the ID and the retardation of flame appearance. The prolonged ID is conducive to improving the uniformity of the air-fuel mixture, resulting in a lower diffusion combustion rate and reducing the concentration and temperature gradients of the combustion process. The cracking reactions of fuels are less likely to take place, leading to reductions in soot generation, diffusion flame area and luminosity. The dilution and the chemical equilibrium closer to reactants caused by external EGR lead to a reduction of the combustion rate, which could also reduce the in-cylinder temperature and inhibit the generation of soot. According to **Fig.11**, as the external EGR rate increases, the flame luminosity along the cylinder wall decreases. This is caused by the strong airflow near the cylinder wall, which helps the mutual diffusion and air-fuel mixing. The fuel around the cylinder axis with insufficient injection pressure and airflow intensity suffers from poor atomization and a slow mixing rate, so the flame near the cylinder axis does not fade away until the EGR rate reaches 20%.

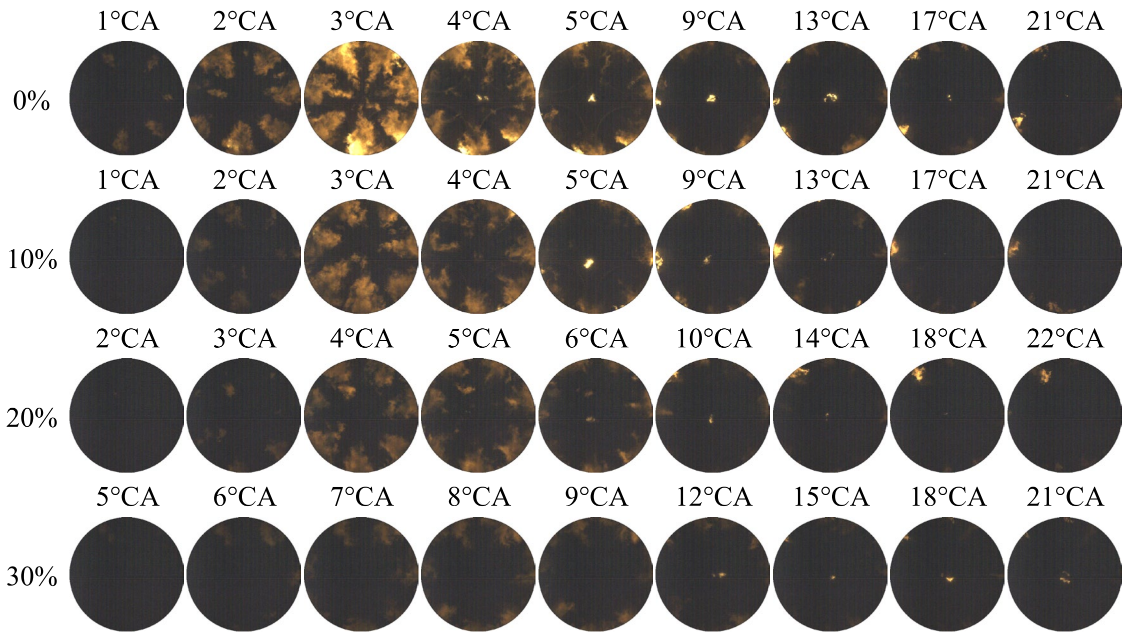

Fig. 11. Effects of external EGR rates on the history of BF flame development.

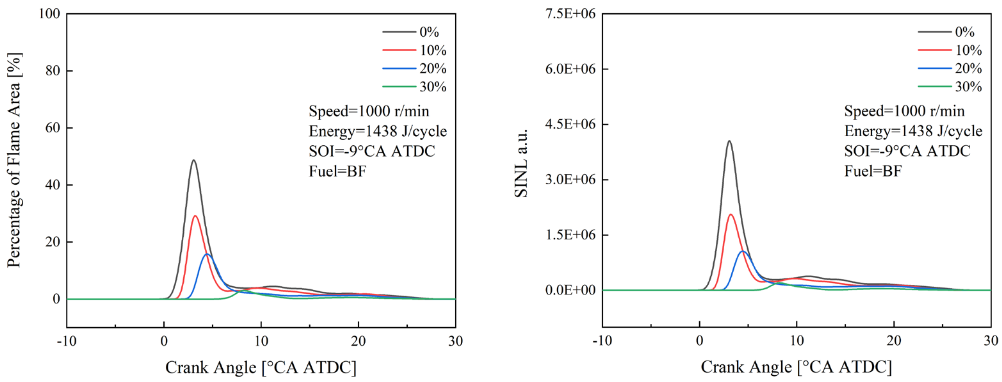

(a) Percentage of flame area (b) SINL

Fig. 12. Effects of external EGR rates on BF flame area and luminosity.

Fig. 13 and **Fig. 14** show the BF flame development and flame characteristics under different internal EGR rates. Unlike the external EGR, it shows an effect of inhibition first and then promotion on the flame area and luminosity as the internal EGR rate increases. When the internal EGR rate is low (NVOA=40°CA), the flame area and luminosity are significantly lower compared with those at the original valve timing (NVOA=-28°CA), and the timing of flame appearance is significantly delayed. As the NVOA reaches 60°CA, the flame area, SINL and the timing of the flame appearance are similar to those of the original valve timing. As the internal EGR rate is increased further, a significant promotion of the ignition process is shown. When NVOA=120°CA, the ID is shorter than that of the original valve timing obviously, resulting in insufficient air-fuel mixing. These changes are very unfavorable to the control of soot emission, therefore making the flame area percentage and SINL almost twice that of the original valve timing. Li et al. suggested that internal EGR could affect the combustion process in two ways: the dilution effect of exhaust gas with higher specific heat, and in contrast, the heating effect of high-temperature residual gas [80]. Under the lower rates of internal EGR, less exhaust gas is trapped and the heating effect on the in-cylinder temperature is weaker, the inhibition effect takes the leading role. As the internal EGR rate increases, the heating effect increases significantly, and the promotion effect becomes dominant gradually. In addition, the implementation of internal EGR requires an alteration of valve timing away from its optimal value, resulting in decreases in the volumetric efficiency and the amount of fresh air, so the heating effect is additionally enhanced. Accordingly, to restrain the in-cylinder temperature using internal EGR, an optimal internal EGR rate is supposed to be found, and an excessive internal EGR rate will lead to further deterioration of combustion.

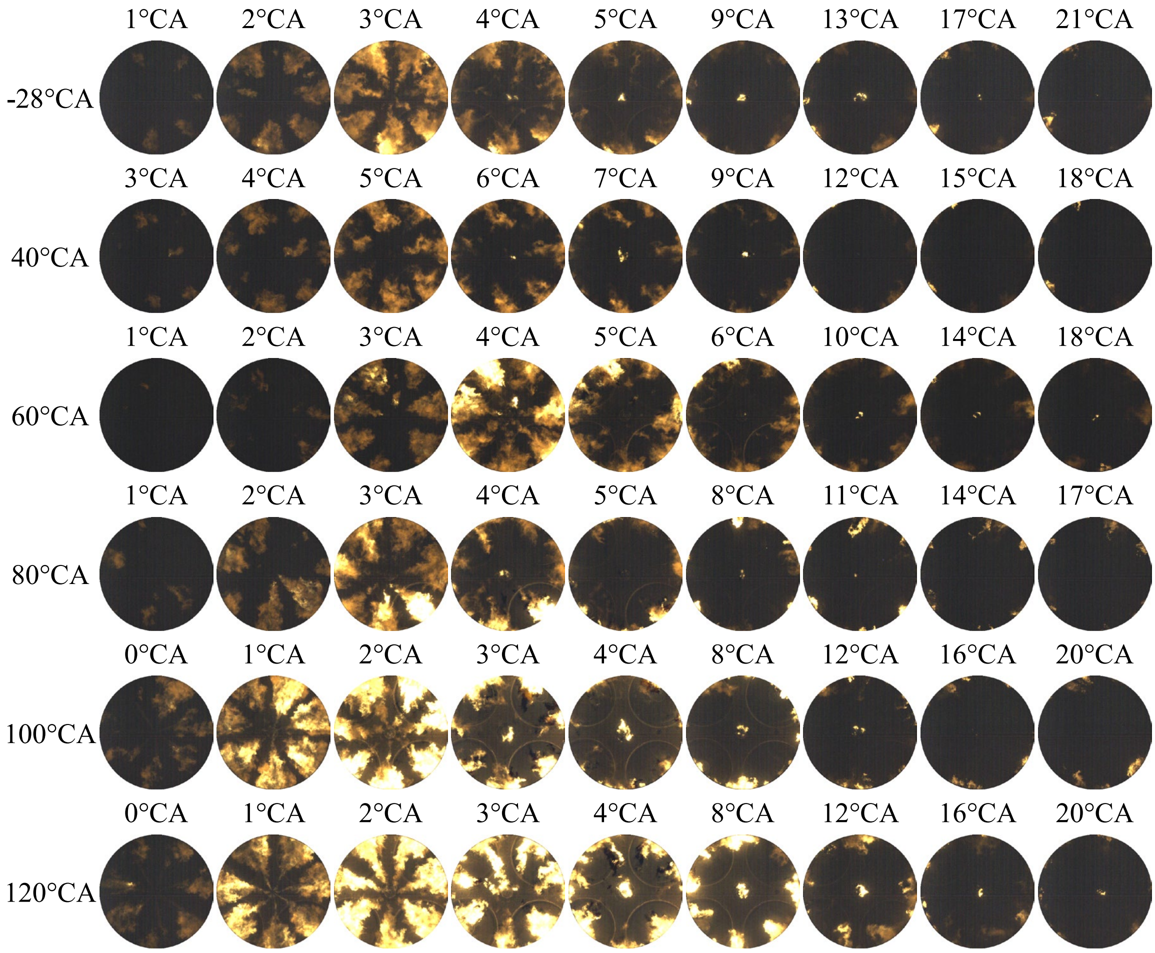

Fig. 13. Effects of internal EGR rates on the history of BF flame development.

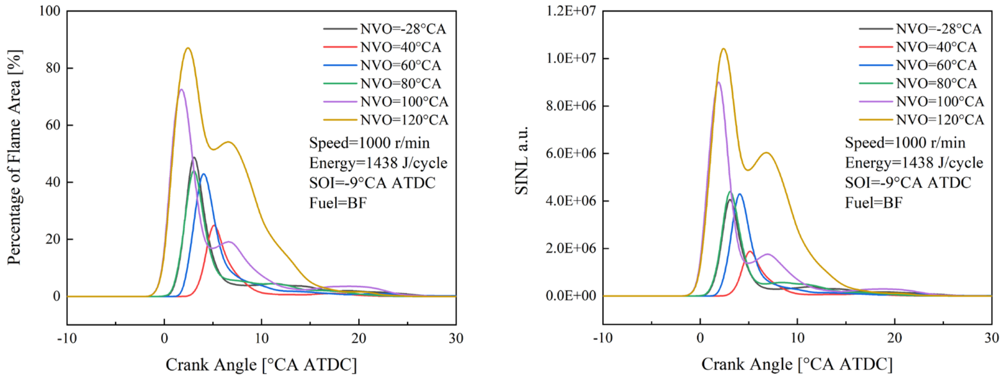

(a) Percentage of flame area (b) SINL

Fig. 14. Effects of internal EGR rates on BF flame area and luminosity.

Fig. 15 shows the distributions of the in-cylinder temperature field of BF at different external EGR rates. As shown in the figure, with the increase of external EGR rate, the total number of high-temperature pixels decreases generally, the pixels with temperatures > 1600 K almost disappear, and the timing of high-temperature region appearance is delayed. External EGR could effectively reduce the proportion of diffusion combustion while suppressing the intensity of the combustion process, thus avoiding local fuel-rich combustion and the temperature range in which soot is generated significantly, providing favorable conditions for the control of soot emission. However, under high-ratio external EGRs, the in-cylinder temperature is suppressed significantly, and the combustion process is delayed excessively, which negatively affects the economy obviously.

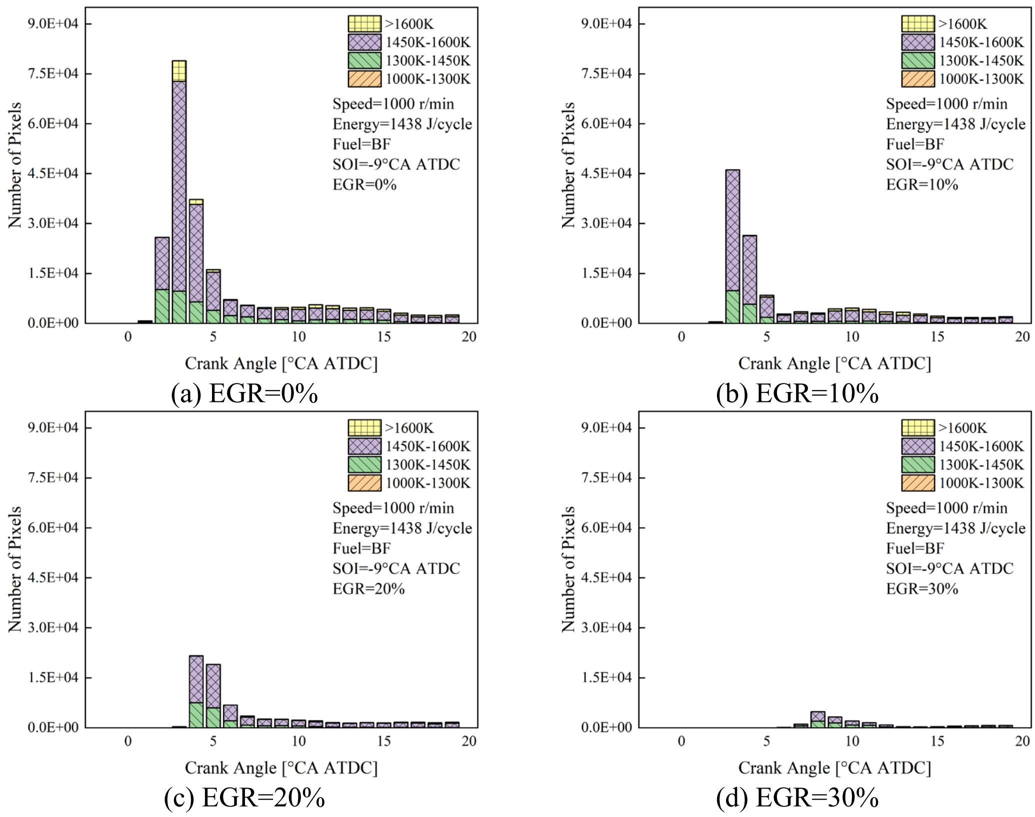

Fig. 15. The cumulative histograms of temperature distribution for different external EGR rates.

The distributions of the in-cylinder temperature field of BF under different internal EGR rates are shown in **Fig. 16**. Since the lower internal EGR rates could prolong the ID appropriately and provide a sufficient air-fuel mixing process, the gradients of in-cylinder concentration and temperature are reduced, resulting in fewer high-temperature pixels when NVOA=40°CA. As the internal EGR rate increases, the promotion effect of internal EGR on in-cylinder temperature gradually dominates. When the NVOA exceeds 80˚CA, the high-temperature combustion phenomenon is more obvious compared to the original valve timing, and the long-lasting high-temperature pixels during the combustion process indicate that the combustion process is prolonged overly. Meanwhile, the excessive heat transfer between the gas and the cylinder wall leads to a decrease in thermal efficiency. Additionally, the over-proportioning of diffusion combustion caused by a high ratio of internal EGR leads to significant increases in the number of high-temperature pixels above 1600 K, which do not contribute to the control of soot emission.

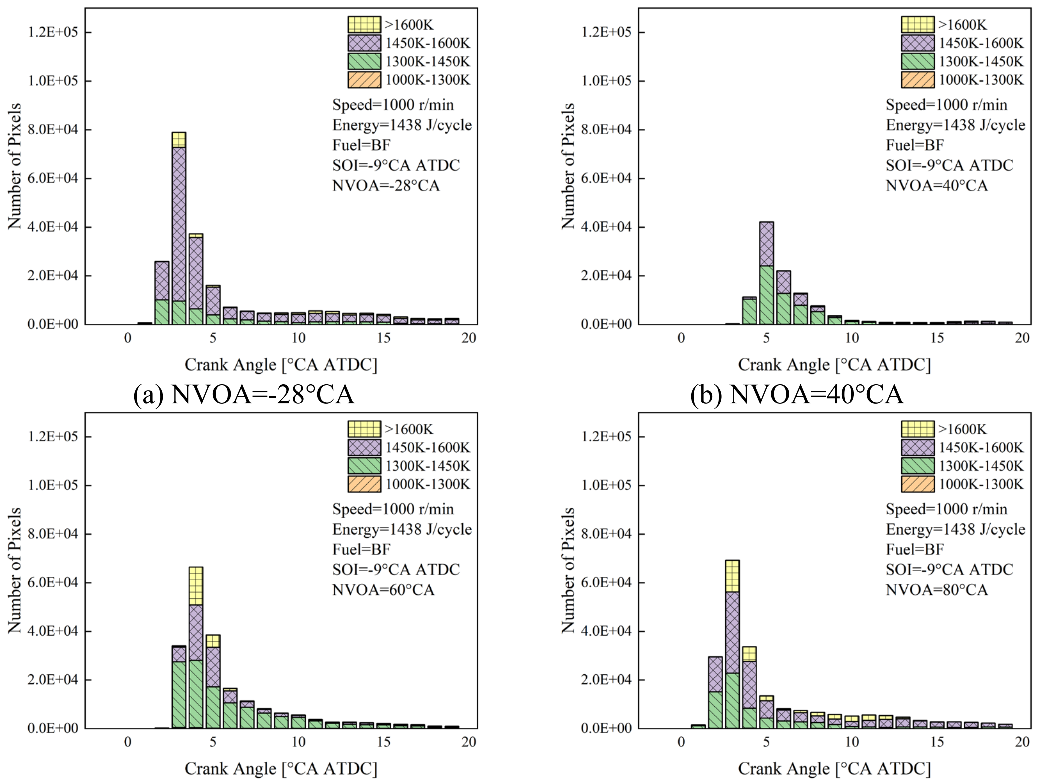

(a) NVOA=-28°CA (b) NVOA=40°CA

(c) NVOA=60°CA (d) NVOA=80°CA

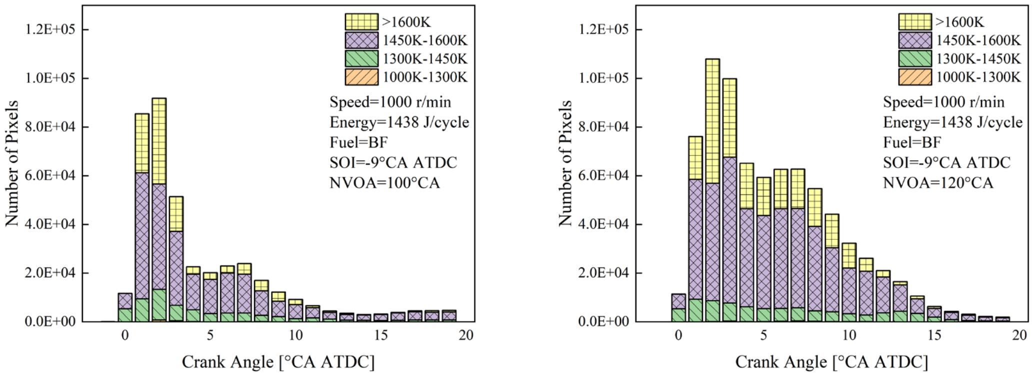

(e) NVOA=100°CA (f) NVOA=120°CA

Fig. 16. The cumulative histograms of temperature distribution for different internal EGR rates.

The effect of external EGR on the KL factor field distribution of BF fuel is shown in **Fig. 17**. Under the combined effect of external EGR and the addition of n-butanol, the improved air-fuel mixing process leads to a lower diffusive combustion rate as well as lower gradients of in-cylinder temperature and concentration. Therefore, the local high-temperature fuel-rich combustion problem is alleviated, resulting in a significant reduction of KL factor. Although the soot KL factor is reduced significantly with a high ratio of external EGR, the delayed timing and the lowered amount of soot generation indicate a reduced thermal efficiency.

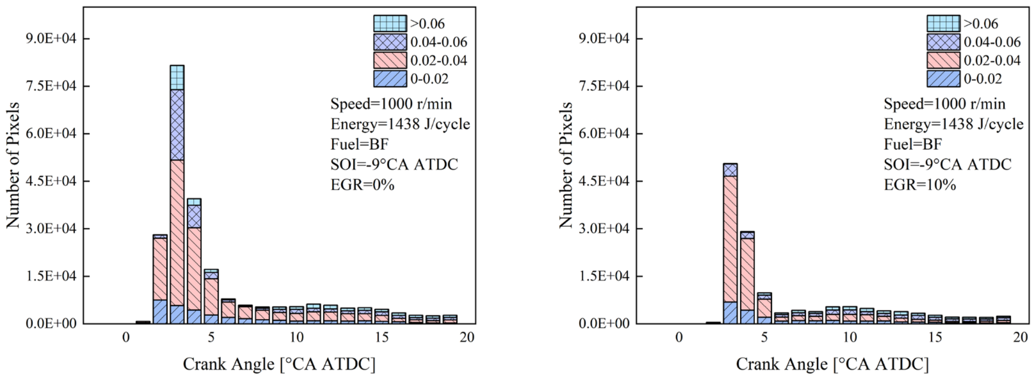

(a) EGR=0% (b) EGR=10%

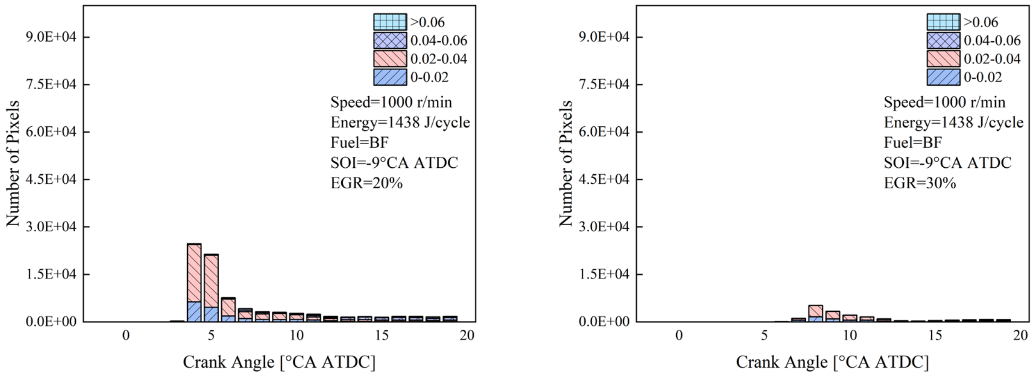

(c) EGR=20% (d) EGR=30%

Fig. 17. The cumulative histograms of soot KL factor distribution for different external EGR rates.

The effect of internal EGR on the KL factor field distribution of BF fuel is shown in **Fig. 18**. Since the low rate of internal EGR could effectively restrain the high-temperature combustion and break the conditions of soot generation, the KL factor decreases significantly and the timing of soot generation is postponed remarkably. As the internal EGR rate increases, the inhibitory effect is gradually transformed into a facilitating effect, the insufficient air-fuel mixing leads to an increased KL factor and the advance of soot generation timing. When the NVOA> 80˚CA, as a result of deteriorated combustion and excessive in-cylinder concentration and temperature gradients, the pre-inhibition and later oxidation effects of internal EGR on soot are weakened, resulting in a significantly higher KL factor compared to the ones with the original valve timing. According to the previous simulation study by our group, the amounts of trapped residual gas at the NVOAs of 60°CA and 100°CA are approximately the same as the amounts of exhaust gas introduced under 10% and 20% external EGRs, respectively. Under the conditions of 10% external EGR and NVOA=60°CA, it shows that the inhibiting effect of internal EGR is weaker than the effect of external EGR at the current condition. Under 20% external EGR and NVOA=100°CA operating conditions, the external EGR maintains a strong inhibitory effect, while the promotion effect exhibited by the internal EGR is rather more significant than its inhibitory effect. The following factors are responsible for this difference. Firstly, in this study, the trapped high-temperature gas has a stronger heating effect than the gas introduced by external EGR, especially under conditions of high EGR ratios. Secondly, the trapped gas has a lower specific heat because of the lower proportion of triatomic gas, and it has a certain reaction activity, leading to a weaker inhibitory effect. The significant impact of the temperature of the EGR gas on the combustion process was also emphasized in reference [79]. Finally, internal EGR leads to an incomplete and insufficient gas exchange process and a reduction of in-cylinder charge [46,81], which further aggravates the heating effect of residual gas and local fuel-rich phenomenon. In contrast, with external EGR, due to the low engine load and relatively high φ_a in this test, the in-cylinder oxygen is sufficient to inhibit soot generation. It must be noted that both internal and external EGR cause severe deterioration of the combustion process when a high EGR rate is adopted. The large proportion of external EGR causes excessively low in-cylinder temperatures and delayed heat release processes, resulting in poor combustion timeliness and stability. The large proportion of internal EGR leads to advanced ignition timing and insufficient air-fuel mixing significantly, which also causes unstable combustion and extensive soot generation. In addition, the negative impact of the introduction of EGR on energy availability deserves attention, as confirmed by the previous exergy assessment [82].

Therefore, in practice, both the internal and external EGR rates have to be controlled strictly.

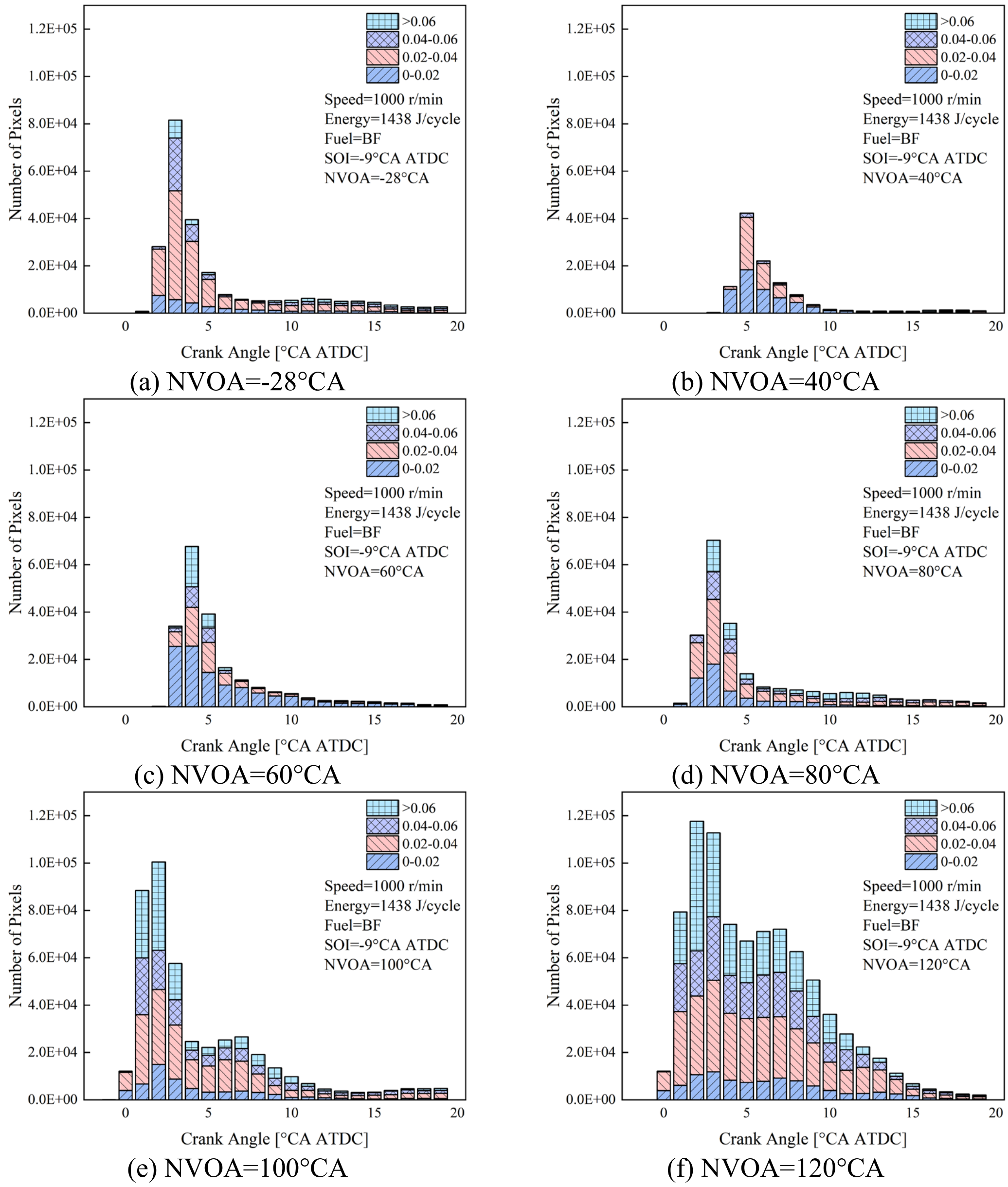

Fig. 18. The cumulative histograms of soot KL factor distribution for different internal EGR rates.

4 Conclusions

In this study, an optical diagnostic study was conducted on the combustion and soot generation history of FT synthetic diesel and its oxygenated blends under different EGR introducing schemes based on a self-built optical engine. The findings of the study can be summarized as follows:

1. The additions of n-butanol, $PODE_3$, and DMC could directly inhibit generation and promote later oxidation of soot via the oxygen-carrying properties to varying degrees, and adjust the physicochemical properties of blended fuels in various ways to promote air-fuel mixing and thus control the generation of soot. Blending oxygenated fuels with FT synthetic diesel could reduce the in-cylinder flame area and luminosity. For oxygenated blends, the local high-temperature fuel-rich combustion phenomenon is alleviated in different degrees, and the KL factors of soot are reduced. Among the three oxygenated fuels, n-butanol exhibits the strongest ability for soot reduction, followed by $PODE_3$ and DMC.

2. The external EGR shows an inhibitory effect on the ignition and combustion processes. As the external EGR rate increases, the combustion rate is decreased, the heat release process of combustion is delayed, the in-cylinder flame area and luminosity are reduced, and the in-cylinder temperature and KL factor are lowered. Because of the minor effect of external EGR on the gas exchange process and the low engine load, the phenomenon of local fuel-rich combustion under a high ratio of external EGR is not obvious in this test.

3. As the internal EGR rate increases, it shows the effect of inhibiting first and then promoting on the ignition and combustion processes. Low-ratio internal EGR could reduce the reaction rate, diffusion flame area and luminosity, as well as the in-cylinder temperature and KL factor. The heating effect of the high-ratio internal EGR shortens the ID significantly, resulting in insufficient air-fuel mixing and obvious increases in

the in-cylinder temperature and KL factor.

4. For EGR schemes with the same introduced amounts, the pure CO_2 from external EGR has a stronger inhibiting effect on the heat release process than the effect of residual gas trapped by internal EGR. In practice, both high ratios of internal and external EGR lead to an excessive deterioration of combustion and a decrease in combustion stability and therefore need to be strictly controlled. The strategy of properly proportioned internal/external EGR with oxygenated fuel additives could effectively optimize the combustion process of FT synthetic diesel and expand the range of high-efficiency-clean-combustion.

Notes

The authors declare no competing financial interest.

Acknowledgments

This work was supported by the National Natural Science Foundation of China (Project code: 52202470); Jilin Province Natural Science Foundation (Project code: 20220101205JC, 20220101212JC); Jilin Province Specific Project of Industrial Technology Research & Development (Project code: 2020C025-2); Free Exploration Project of Changsha Automotive Innovation Research Institute of Jilin University (Project code: CAIRIZT20220202); Horizon 2020 MSCA (Project code: H2020-MSCA-RISE-778104-ThermaSMART); Graduate Innovation Fund of Jilin University (2023CX076).

References

[1] Allen CD, Macalady AK, Chenchouni H, Bachelet D, McDowell N, Vennetier

M, et al. A global overview of drought and heat-induced tree mortality reveals emerging climate change risks for forests. FOREST ECOLOGY AND MANAGEMENT 2010;259(4):660-84. https://doi.org/10.1016/j.foreco.2009.09.001.

[2] Oda T, Maksyutov S, Andres RJ. The Open-source Data Inventory for Anthropogenic CO2, version 2016 (ODIAC2016): a global monthly fossil fuel CO2 gridded emissions data product for tracer transport simulations and surface flux inversions. EARTH SYSTEM SCIENCE DATA 2018;10(1):87-107. https://doi.org/10.5194/essd-10-87-2018.

[3] Verhelst S, Turner JWG, Sileghem L, Vancoillie J. Methanol as a fuel for internal combustion engines. PROGRESS IN ENERGY AND COMBUSTION SCIENCE 2019;70:43-88. https://doi.org/10.1016/j.pecs.2018.10.001.

[4] Rogelj J, den Elzen M, Hohne N, Fransen T, Fekete H, Winkler H, et al. Paris Agreement climate proposals need a boost to keep warming well below 2 degrees C. NATURE 2016;534(7609):631-9. https://doi.org/10.1038/nature18307.

[5] Fasihi M, Efimova O, Breyer C. Techno-economic assessment of CO2 direct air capture plants. JOURNAL OF CLEANER PRODUCTION 2019;224:957-80. https://doi.org/10.1016/j.jclepro.2019.03.086.

[6] Xu YY, Ramanathan V. Well below 2 degrees C: Mitigation strategies for avoiding dangerous to catastrophic climate changes. PROCEEDINGS OF THE NATIONAL ACADEMY OF SCIENCES OF THE UNITED STATES OF AMERICA 2017;114(39):10315-23. https://doi.org/10.1073/pnas.1618481114.

[7] Williams JH, Jones RA, Haley B, Kwok G, Hargreaves J, Farbes J, et al.

Carbon-Neutral Pathways for the United States. AGU ADVANCES 2021;2(1). https://doi.org/10.1029/2020AV000284.

[8] Chen JW, Cui HJ, Xu YY, Ge QS. Long-term temperature and sea-level rise stabilization before and beyond 2100: Estimating the additional climate mitigation contribution from China's recent 2060 carbon neutrality pledge. ENVIRONMENTAL RESEARCH LETTERS 2021;16(7). https://doi.org/10.1088/1748-9326/ac0cac.

[9] Zhao JY, Yu YD, Ren HT, Makowski M, Granat J, Nahorski Z, et al. How the power-to-liquid technology can contribute to reaching carbon neutrality of the China's transportation sector? ENERGY 2022;261. https://doi.org/10.1016/j.energy.2022.125058.

[10] Li JX, Zhu X, Djilali N, Yang Y, Ye DD, Chen R, et al. Comparative well-to-pump assessment of fueling pathways for zero-carbon transportation in China: Hydrogen economy or methanol economy? RENEWABLE & SUSTAINABLE ENERGY REVIEWS 2022;169. https://doi.org/10.1016/j.rser.2022.112935.

[11] Mat SC, Idroas MY, Teoh YH, Hamid MF, Sharudin H, Pahmi M. Optimization of ternary blends among refined palm oil-hexanol-melaleuca cajuputi oil and engine emissions analysis of the blends. RENEWABLE ENERGY 2022;196:451-61. https://doi.org/10.1016/j.renene.2022.07.018.

[12] Varuvel EG, Thiyagarajan S, Sonthalia A, Prakash T, Awad S, Aloui F, et al. Some studies on reducing carbon dioxide emission from a CRDI engine with hydrogen and a carbon capture system. INTERNATIONAL JOURNAL OF HYDROGEN ENERGY 2022;47(62):26746-57. https://doi.org/10.1016/j.ijhydene.2021.12.174.

[13] Abad AV, Dodds PE. Green hydrogen characterisation initiatives: Definitions, standards, guarantees of origin, and challenges. ENERGY POLICY 2020;138. https://doi.org/10.1016/j.enpol.2020.111300.

[14] Zincir B. Environmental and economic evaluation of ammonia as a fuel for short-sea shipping: A case study. INTERNATIONAL JOURNAL OF HYDROGEN ENERGY 2022;47(41):18148-68. https://doi.org/10.1016/j.ijhydene.2022.03.281.

[15] Ueckerdt F, Bauer C, Dirnaichner A, Everall J, Sacchi R, Luderer G. Potential and risks of hydrogen-based e-fuels in climate change mitigation. NATURE CLIMATE CHANGE 2021;11(5):384-+. https://doi.org/10.1038/s41558-021-01032-7.

[16] Lindstad E, Lagemann B, Rialland A, Gamlem GM, Valland A. Reduction of maritime GHG emissions and the potential role of E-fuels. TRANSPORTATION RESEARCH PART D-TRANSPORT AND ENVIRONMENT 2021;101. https://doi.org/10.1016/j.trd.2021.103075.

[17] Fleisch TH, Basu A, Sills RA. Introduction and advancement of a new clean global fuel: The status of DME developments in China and beyond. JOURNAL OF NATURAL GAS SCIENCE AND ENGINEERING 2012;9:94-107. https://doi.org/10.1016/j.jngse.2012.05.012.

[18] Pastor JV, Garcia A, Mico C, Lewiski F. An optical investigation of Fischer-Tropsch diesel and Oxymethylene dimethyl ether impact on combustion process for CI engines. APPLIED ENERGY 2020;260. https://doi.org/10.1016/j.apenergy.2019.114238.

[19] van Vliet OPR, Faaij APC, Turkenburg WC. Fischer-Tropsch diesel

production in a well-to-wheel perspective: A carbon, energy flow and cost analysis. ENERGY CONVERSION AND MANAGEMENT 2009;50(4):855-76. https://doi.org/10.1016/j.enconman.2009.01.008.

[20] Szybist JP, Kirby SR, Boehman AL. NOx emissions of alternative diesel fuels: A comparative analysis of biodiesel and FT diesel. ENERGY & FUELS 2005;19(4):1484-92. https://doi.org/10.1021/ef049702q.

[21] Gill SS, Tsolakis A, Dearn KD, Rodriguez-Fernandez J. Combustion characteristics and emissions of Fischer-Tropsch diesel fuels in IC engines. PROGRESS IN ENERGY AND COMBUSTION SCIENCE 2011;37(4):503-23. https://doi.org/10.1016/j.pecs.2010.09.001.

[22] Shi JH, Wang T, Zhao Z, Yang TT, Zhang ZW. Experimental Study of Injection Parameters on the Performance of a Diesel Engine with Fischer-Tropsch Fuel Synthesized from Coal. ENERGIES 2018;11(12). https://doi.org/10.3390/en11123280.

[23] Zhang H, Sun WC, Guo L, Yan YY, Li J, Lin SD, et al. An experimental study of using coal to liquid (CTL) and diesel as pilot fuels for gasoline dual-fuel combustion. FUEL 2021;289. https://doi.org/10.1016/j.fuel.2020.119962.

[24] Lou DM, Peng Y, Hu ZY, Tai PQ, Ieee. Characteristics of Modal Particulate Emission on Diesel Car by Coal-to-Liquid Blends. 2013 INTERNATIONAL CONFERENCE ON MATERIALS FOR RENEWABLE ENERGY AND ENVIRONMENT (ICMREE), VOLS 1-3. 2013:261-4. https://doi.org/10.1109/ICMREE.2013.6893661.

[25] Jin C, Mao B, Dong F, Liu XL, Yang Y, Chen P, et al. Effects of Indirect and

Direct Coal-to-Liquid Fuel on Combustion, Performance, and Emissions in a Six-Cylinder Heavy-Duty Diesel Engine. JOURNAL OF ENERGY ENGINEERING 2018;144(3). https://doi.org/10.1061/(ASCE)EY.1943-7897.0000531.

[26] Uchida N, Sakata I, Kitano K, Okabe N, Sakamoto Y. Simultaneous improvement in both exhaust emissions and fuel consumption by means of Fischer-Tropsch diesel fuels. INTERNATIONAL JOURNAL OF ENGINE RESEARCH 2014;15(1):20-36. https://doi.org/10.1177/1468087412456528.

[27] Sajjad H, Masjuki HH, Varman M, Kalam MA, Arbab MI, Imtenan S, et al. Comparative study of gas-to-liquid fuel, B5 diesel and their blends with respect to fuel properties, engine performance and exhaust emissions. RSC ADVANCES 2014;4(84):44529-36. https://doi.org/10.1039/c4ra06837h.

[28] Fayad MA, Tsolakis A, Martos FJ. Influence of alternative fuels on combustion and characteristics of particulate matter morphology in a compression ignition diesel engine. RENEWABLE ENERGY 2020;149:962-9. https://doi.org/10.1016/j.renene.2019.10.079.

[29] Zhang H, Sun WC, Guo L, Yan YY, Sun Y, Zeng WP, et al. Optical diagnostic study of coal-to-liquid/butanol blend and dual-fuel combustion of a CI engine. FUEL 2022;320. https://doi.org/10.1016/j.fuel.2022.123978.

[30] Dai YL, Pei YQ, Qin J, Zhang JY, Li YL. Experimental Study of Coal Liquefaction Diesel Combustion and Emissions. ADVANCES IN ENERGY SCIENCE AND TECHNOLOGY, PTS 1-4. 291-294. 2013:1914-9. https://doi.org/10.4028/www.scientific.net/AMM.291-294.1914.

[31]Nabi MN, Zare A, Hossain FM, Bodisco TA, Ristovski ZD, Brown RJ. A parametric study on engine performance and emissions with neat diesel and diesel-butanol blends in the 13-Mode European Stationary Cycle. ENERGY CONVERSION AND MANAGEMENT 2017;148:251-9. https://doi.org/10.1016/j.enconman.2017.06.001.

[32]Chen Z, Liu JP, Han ZY, Du B, Liu Y, Lee C. Study on performance and emissions of a passenger-car diesel engine fueled with butanol-diesel blends. ENERGY 2013;55:638-46. https://doi.org/10.1016/j.energy.2013.03.054.

[33]Yang JC, Jiang Y, Karavalakis G, Johnson KC, Kumar S, Cocker DR, et al. Impacts of dimethyl carbonate blends on gaseous and particulate emissions from a heavy-duty diesel engine. FUEL 2016;184:681-8. https://doi.org/10.1016/j.fuel.2016.07.053.

[34]Pan MZ, Qian WW, Zheng ZY, Huang R, Zhou XR, Huang HZ, et al. The potential of dimethyl carbonate (DMC) as an alternative fuel for compression ignition engines with different EGR rates. FUEL 2019;257. https://doi.org/10.1016/j.fuel.2019.115920.

[35]Liu HY, Wang Z, Wang JX, He X, Zheng YY, Tang Q, et al. Performance, combustion and emission characteristics of a diesel engine fueled with polyoxymethylene dimethyl ethers (PODE3-4)/diesel blends. ENERGY 2015;88:793-800. https://doi.org/10.1016/j.energy.2015.05.088.

[36] Chen H, Huang R, Huang HZ, Pan MZ, Teng WW. Potential improvement in particulate matter's emissions reduction from diesel engine by addition of PODE and

injection parameters. APPLIED THERMAL ENGINEERING 2019;150:591-604. https://doi.org/10.1016/j.applthermaleng.2019.01.026.

[37] Pepiot-Desjardins P, Pitsch H, Malhotra R, Kirby SR, Boehman AL. Structural group analysis for soot reduction tendency of oxygenated fuels. COMBUSTION AND FLAME 2008;154(1-2):191-205. https://doi.org/10.1016/j.combustflame.2008.03.017.

[38] Ramesh A, Ashok B, Nanthagopal K, Pathy MR, Tambare A, Mali P, et al. Influence of hexanol as additive with Calophyllum Inophyllum biodiesel for CI engine applications. FUEL 2019;249:472-85. https://doi.org/10.1016/j.fuel.2019.03.072.

[39] Garcia A, Monsalve-Serrano J, Villalta D, Guzman-Mendoza M. Parametric assessment of the effect of oxygenated low carbon fuels in a light-duty compression ignition engine. FUEL PROCESSING TECHNOLOGY 2022;229. https://doi.org/10.1016/j.fuproc.2022.107199.

[40] Mueller CJ, Boehman AL, Martin GC. An Experimental Investigation of the Origin of Increased NOx Emissions When Fueling a Heavy-Duty Compression-Ignition Engine with Soy Biodiesel. SAE International Journal of Fuels and Lubricants 2009;2(1):789-816. https://doi.org/10.4271/2009-01-1792.

[41] Atmanli A. Comparative analyses of diesel-waste oil biodiesel and propanol, n-butanol or 1-pentanol blends in a diesel engine. FUEL 2016;176:209-15. https://doi.org/10.1016/j.fuel.2016.02.076.

[42] Imtenan S, Masjuki HH, Varman M, Fattah IMR, Sajjad H, Arbab MI. Effect of n-butanol and diethyl ether as oxygenated additives on combustion-emission-performance characteristics of a multiple cylinder diesel engine fuelled with diesel-

jatropha biodiesel blend. ENERGY CONVERSION AND MANAGEMENT 2015;94:84-94. https://doi.org/10.1016/j.enconman.2015.01.047.

[43] Bhowmick P, Jeevanantham AK, Ashok B, Nanthagopal K, Perumal DA, Karthickeyan V, et al. Effect of fuel injection strategies and EGR on biodiesel blend in a CRDI engine. ENERGY 2019;181:1094-113. https://doi.org/10.1016/j.energy.2019.06.014.

[44] Ali SS, De Poures MV, Damodharan D, Gopal K, Augustin VC, Swaminathan MR. Prediction of emissions and performance of a diesel engine fueled with waste cooking oil and C8 oxygenate blends using response surface methodology. JOURNAL OF CLEANER PRODUCTION 2022;371. https://doi.org/10.1016/j.jclepro.2022.133323.

[45] Zhou XR, Qian WW, Pan MZ, Huang R, Xu LL, Yin JC. Potential of n-butanol/diesel blends for CI engines under post injection strategy and different EGR rates conditions. ENERGY CONVERSION AND MANAGEMENT 2020;204. https://doi.org/10.1016/j.enconman.2019.112329.

[46] Duan XB, Liu YQ, Liu JP, Lai MC, Jansons M, Guo GM, et al. Experimental and numerical investigation of the effects of low-pressure, high-pressure and internal EGR configurations on the performance, combustion and emission characteristics in a hydrogen-enriched heavy-duty lean-burn natural gas SI engine. ENERGY CONVERSION AND MANAGEMENT 2019;195:1319-33. https://doi.org/10.1016/j.enconman.2019.05.059.

[47] Zhang WZ, Li X, Huang L, Feng MZ. Experimental study on spray and

evaporation characteristics of diesel-fueled marine engine conditions based on optical diagnostic technology. FUEL 2019;246:454-65. https://doi.org/10.1016/j.fuel.2019.02.065.

[48] Catapano F, Sementa P, Vaglieco BM. Optical characterization of bio-ethanol injection and combustion in a small DISI engine for two wheels vehicles. FUEL 2013;106:651-66. https://doi.org/10.1016/j.fuel.2012.11.064.

[49] Irimescu A, Marchitto L, Merola SS, Tornatore C, Valentino G. Combustion process investigations in an optically accessible DISI engine fuelled with n-butanol during part load operation. RENEWABLE ENERGY 2015;77:363-76. https://doi.org/10.1016/j.renene.2014.12.029.

[50] Williams B, Ewart P, Wang XW, Stone R, Ma HR, Walmsley H, et al. Quantitative planar laser-induced fluorescence imaging of multi-component fuel/air mixing in a firing gasoline-direct-injection engine: Effects of residual exhaust gas on quantitative PLIF. COMBUSTION AND FLAME 2010;157(10):1866-78. https://doi.org/10.1016/j.combustflame.2010.06.004.

[51] Attar MA, Herfatmanesh MR, Zhao H, Cairns A. Experimental investigation of direct injection charge cooling in optical GDI engine using tracer-based PLIF technique. EXPERIMENTAL THERMAL AND FLUID SCIENCE 2014;59:96-108. https://doi.org/10.1016/j.expthermflusci.2014.07.020.

[52] Menkiel B, Donkerbroek A, Uitz R, Cracknell R, Ganippa L. Measurement of in-cylinder soot particles and their distribution in an optical HSDI diesel engine using time resolved laser induced incandescence (TR-LII). COMBUSTION AND FLAME

2012;159(9):2985-98. https://doi.org/10.1016/j.combustflame.2012.03.008.

[53] El Adawy M, Heikal MR, Aziz ARA, Munir S, Siddiqui MI. Effect of Boost Pressure on the In-Cylinder Tumble-Motion of GDI Engine under Steady-State Conditions using Stereoscopic-PIV. JOURNAL OF APPLIED FLUID MECHANICS 2018;11(3):733-42. https://doi.org/10.18869/acadpub.jafm.73.246.28506.

[54] Hult J, Matamis A, Baudoin E, Mayer S, Richter M. Spatiotemporal flame mapping in a large-bore marine diesel engine using multiple high-speed cameras. INTERNATIONAL JOURNAL OF ENGINE RESEARCH 2020;21(4):622-31. https://doi.org/10.1177/1468087419853429.

[55] Guo HJ, Ma X, Li YF, Liang S, Wang Z, Xu HM, et al. Effect of flash boiling on microscopic and macroscopic spray characteristics in optical GDI engine. FUEL 2017;190:79-89. https://doi.org/10.1016/j.fuel.2016.11.043.

[56] Matsui Y, Kamimoto T, Matsuoka S. A Study on the Time and Space Resolved Measurement of Flame Temperature and Soot Concentration in a D. I. Diesel Engine by the Two-Color Method. SAE International; 1979. https://doi.org/10.4271/790491

[57] Matsui Y, Kamimoto T, Matsuoka S. A Study on the Application of the Two–Color Method to the Measurement of Flame Temperature and Soot Concentration in Diesel Engines. SAE International; 1980. https://doi.org/10.4271/800970

[58] Potenza M, Milanese M, Naccarato F, de Risi A. In-cylinder soot concentration measurement by Neural Network Two Colour technique (NNTC) on a GDI engine. COMBUSTION AND FLAME 2020;217:331-45. https://doi.org/10.1016/j.combustflame.2020.03.024.

[59] Merola SS, Sementa P, Tornatore C, Vaglieco BM. Effect of the fuel injection strategy on the combustion process in a PFI boosted spark-ignition engine. ENERGY 2010;35(2):1094-100. https://doi.org/10.1016/j.energy.2009.06.002.

[60] Han YT, Lee KH, Min KD. A study on the measurement of temperature and soot in a constant-volume chamber and a visualized diesel engine using the two-color method. JOURNAL OF MECHANICAL SCIENCE AND TECHNOLOGY 2009;23(11):3114-23. https://doi.org/10.1007/s12206-009-0817-2.

[61] Musculus MPB, Singh S, Reitz RD. Gradient effects on two-color soot optical pyrometry in a heavy-duty DI diesel engine. COMBUSTION AND FLAME 2008;153(1-2):216-27. https://doi.org/10.1016/j.combustflame.2007.10.023.

[62] Lee J, Oh H, Bae C. Combustion process of JP-8 and fossil Diesel fuel in a heavy duty diesel engine using two-color thermometry. FUEL 2012;102:264-73. https://doi.org/10.1016/j.fuel.2012.07.029.

[63] Jeon J, Park S. Effect of injection pressure on soot formation/oxidation characteristics using a two-color photometric method in a compression-ignition engine fueled with biodiesel blend (B20). APPLIED THERMAL ENGINEERING 2018;131:284-94. https://doi.org/10.1016/j.applthermaleng.2017.12.005.

[64] Rakopoulos CD, Rakopoulos DC, Kosmadakis GM, Papagiannakis RG. Experimental comparative assessment of butanol or ethanol diesel-fuel extenders impact on combustion features, cyclic irregularity, and regulated emissions balance in heavy-duty diesel engine. ENERGY 2019;174:1145-57. https://doi.org/10.1016/j.energy.2019.03.063.

[65] Klein D, Pischinger S. Laser-Induced Incandescence Measurements of Tailor-Made Fuels in an Optical Single-Cylinder Diesel Engine. SAE International Journal of Engines 2017;10(3):1143-54. https://doi.org/10.4271/2017-01-0711.

[66] Di Iorio S, Magno A, Mancaruso E, Vaglieco BM. Analysis of the effects of diesel/methane dual fuel combustion on nitrogen oxides and particle formation through optical investigation in a real engine. FUEL PROCESSING TECHNOLOGY 2017;159:200-10. https://doi.org/10.1016/j.fuproc.2017.01.009.

[67] Zhang R, Chen L, Wei HQ, Li JG, Ding Y, Chen R, et al. Experimental investigation on reactivity-controlled compression ignition (RCCI) combustion characteristic of n-heptane/ammonia based on an optical engine. INTERNATIONAL JOURNAL OF ENGINE RESEARCH. https://doi.org/10.1177/14680874221124452.

[68] Shi Q, Li T, Zhang X, Wang B, Zheng M. Measurement of Temperature and Soot (KL) Distributions in Spray Flames of Diesel-Butanol Blends by Two-Color Method Using High-Speed RGB Video Camera. SAE International; 2016. https://doi.org/10.4271/2016-01-2190.

[69] Kawamura K, Saito A, Yaegashi T, Iwashita Y. Measurement of Flame Temperature Distribution in Engines by Using a Two-Color High Speed Shutter TV Camera System. SAE Transactions 1989;98:434-41. https://doi.org/10.4271/890320.

[70] Rakopoulos DC, Rakopoulos CD, Giakoumis EG, Papagiannakis RG. Evaluating Oxygenated Fuel's Influence on Combustion and Emissions in Diesel Engines Using a Two-Zone Combustion Model. JOURNAL OF ENERGY ENGINEERING 2018;144(4). https://doi.org/10.1061/(ASCE)EY.1943-7897.0000556.

[71] Liu JH, Wang LJ, Wang P, Sun P, Liu HF, Meng ZW, et al. An overview of polyoxymethylene dimethyl ethers as alternative fuel for compression ignition engines. FUEL 2022;318. https://doi.org/10.1016/j.fuel.2022.123582.

[72] Dec JE. A Conceptual Model of DI Diesel Combustion Based on Laser-Sheet Imaging*. SAE International 1997. https://doi.org/10.4271/970873.

[73] Neely GD, Sasaki S, Huang Y, Leet JA, Stewart DW. New Diesel Emission Control Strategy to Meet US Tier 2 Emissions Regulations. SAE Transactions 2005;114:512-24. https://doi.org/10.4271/2005-01-1091.

[74] Park SW, Reitz RD. Numerical study on the low emission window of homogeneous charge compression ignition diesel combustion. COMBUSTION SCIENCE AND TECHNOLOGY 2007;179(11):2279-307. https://doi.org/10.1080/00102200701484142.

[75] Fang J, Liu Y, Wang K, Shah HR, Mu SJ, Lang XQ, et al. Sooting tendency analysis of oxygenate-diesel blended fuels by the affecting indicators of carbon number, oxygen content and H/C ratio. FUEL 2021;290. https://doi.org/10.1016/j.fuel.2020.119789.

[76] Tan YR, Botero ML, Sheng Y, Dreyer JAH, Xu R, Yang WM, et al. Sooting characteristics of polyoxymethylene dimethyl ether blends with diesel in a diffusion flame. FUEL 2018;224:499-506. https://doi.org/10.1016/j.fuel.2018.03.051.

[77] Huang HZ, Li ZJ, Teng WW, Zhou CZ, Huang R, Liu HF, et al. Influence of n-butanol-diesel-PODE3-4 fuels coupled pilot injection strategy on combustion and emission characteristics of diesel engine. FUEL 2019;236:313-24.

https://doi.org/10.1016/j.fuel.2018.09.051.

[78] Maiboom A, Tauzia X, Hetet JF. Experimental study of various effects of exhaust gas recirculation (EGR) on combustion and emissions of an automotive direct injection diesel engine. ENERGY 2008;33(1):22-34. https://doi.org/10.1016/j.energy.2007.08.010.

[79] Hountalas DT, Mavropoulos GC, Binder KB. Effect of exhaust gas recirculation (EGR) temperature for various EGR rates on heavy duty DI diesel engine performance and emissions. ENERGY 2008;33(2):272-83. https://doi.org/10.1016/j.energy.2007.07.002.

[80] Li XL, Chen HY, Zhu ZY, Zhen H. Study of combustion and emission characteristics of a diesel engine operated with dimethyl carbonate. ENERGY CONVERSION AND MANAGEMENT 2006;47(11-12):1438-48. https://doi.org/10.1016/j.enconman.2005.08.021.

[81] Deng BL, Yang J, Zhang DM, Feng RH, Fu JQ, Liu JP, et al. The challenges and strategies of butanol application in conventional engines: The sensitivity study of ignition and valve timing. APPLIED ENERGY 2013;108:248-60. https://doi.org/10.1016/j.apenergy.2013.03.018.

[82] Rakopoulos DC, Rakopoulos CD, Kosmadakis GM, Giakoumis EG. Exergy assessment of combustion and EGR and load effects in DI diesel engine using comprehensive two-zone modeling. ENERGY 2020;202. https://doi.org/10.1016/j.energy.2020.117685.